IEEE Photonics Journal
An IEEE Photonics Society Publication

Open Access

The Lattice Structure and Optical Properties of Neodymium-Doped Gadolinium Vanadate Crystals Induced by Ion Irradiation

Volume 9, Number 3, June 2017

Mei Qiao
Tiejun Wang
Honglian Song
Jing Zhang
Yong Liu
Peng Liu
Huaijin Zhang
Xuelin Wang

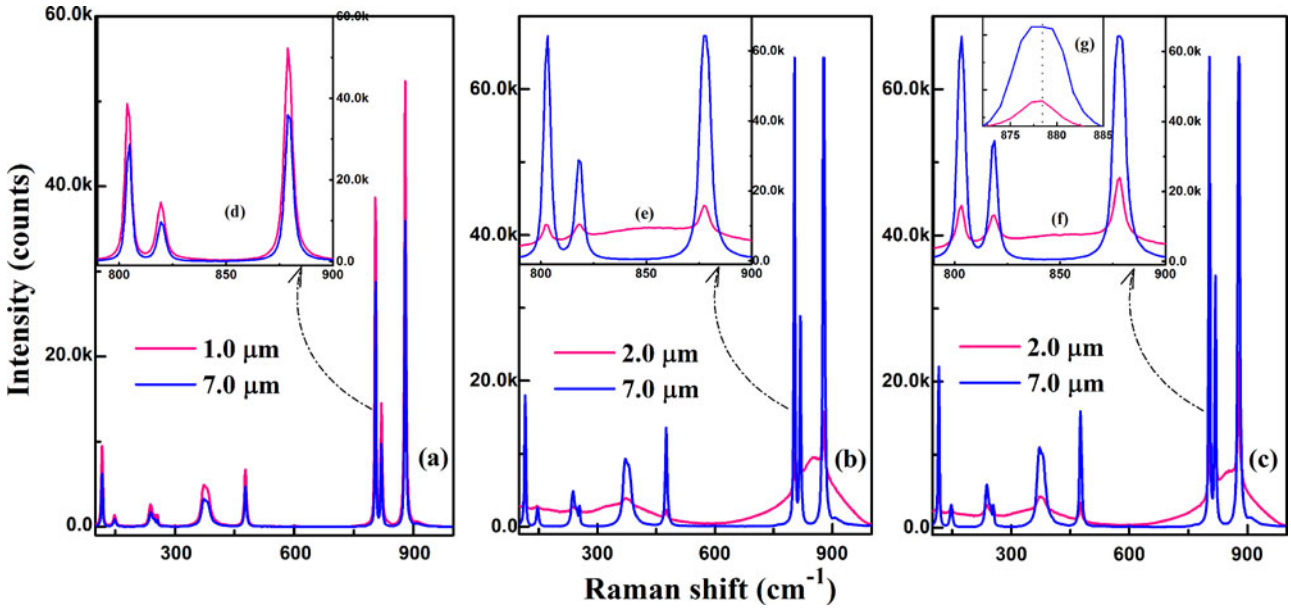

DOI: 10.1109/JPHOT.2017.2701888
1943-0655 © 2017 IEEE

The Lattice Structure and Optical Properties of Neodymium-Doped Gadolinium Vanadate Crystals Induced by Ion Irradiation

Mei Qiao, Tiejun Wang, Honglian Song, Jing Zhang, Yong Liu, Peng Liu, Huaijin Zhang, and Xuelin Wang

School of Physics, State Key Laboratory of Crystal Materials and Key Laboratory of Particle Physics and Particle Irradiation (MOE), Shandong University, Jinan 250100, China

DOI:10.1109/JPHOT.2017.2701888

Manuscript received April 22, 2017; accepted May 3, 2017. Date of current version May 25, 2017. This work was support by the National Natural Science Foundation of China under Grant U1432120 and in part by the Taishan Scholar Program of Shandong. Corresponding Author: Xue-Lin Wang (e-mail: xuelinwang@sdu.edu.cn).

Abstract: In recent times, the neodymium-doped gadolinium vanadate (Nd:$GdVO_4$) crystal has attracted significant attention as one of the most valuable functional materials, but its lattice structure can be easily modified in an irradiation environment, which determines its related optical properties and affects the performance of devices based on the Nd:$GdVO_4$ crystal. The near-surface lattice structure change and damage are studied through the displacement per atom (dpa), X-Ray diffraction, hardness and elastic (Young's) modulus, and micro-Raman spectroscopy techniques. We discover that the intensity and peak position of micro-Raman have obvious changes between waveguide and substrate region in Nd:$GdVO_4$ crystal. The related optical properties induced by the structural changes, including the absorption bands and refractive index profiles, are investigated. A new absorption peak was observed after irradiation of the Nd:$GdVO_4$ crystals by C^{3+} ions. Thus, waveguide optical-coupling techniques identified that the ion- irradiated Nd:$GdVO_4$ crystal can support single-mode or multimode propagation at 633 nm. The fabricated waveguide structures emerge as promising candidate for photonic design and integrated optical devices, which will have a huge application prospect in multimedia and internet.

Index Terms: Fabrication and characterization, optoelectronic materials, spectroscopy, waveguides.

1. Introduction

$GdVO_4$, which has four chemical formulae per unit cell ($z = 4$), is a tetragonal crystal system with space group $I_{41}/_{amd}$ (JCPDS $-$ 17 $-$ 0260), which is the same as yttrium vanadate. In recent years, neodymium-doped crystals have attracted significant attention due to their excellent lasing properties [1], [2]. Nd:$GdVO_4$ is an efficient laser material for diode pumping compared with neodymium-doped yttrium aluminum garnet and neodymium-doped yttrium vanadate; moreover, among various Nd-doped laser media, Nd:$GdVO_4$ is one of the most attractive, and it has been extolled in recent years [3]–[7]. As an oxide phosphor, Nd:$GdVO_4$ has the advantage of a higher chemical stability. In addition, its absorption band is approximately 1.6 nm at 808.4 nm, which is

TABLE 1
Details of the ION-Irradiated Nd:$GdVO_4$ Samples

Sample	Irradiated ion	Energy (keV)	Fluences (ions/cm^2)
S0	-	-	-
S1	H	460	5.6×10^{16}
S2	C^{3+}	6000	1.0×10^{15}
S3	C^{3+}	6000	3.0×10^{15}

a good match with the emission band of a GaAlAs laser diode [8]. Nd:$GdVO_4$ is also an excellent gain medium due to its high thermal conductivity and absorption coefficient [9]–[12]. The excellent spectroscopic properties, such as the large emission cross- section, and high Raman gain, have also been proven in previous studies [13], [14]. Up to now, femtosecond laser direct writing has been used to fabricate channel waveguides successfully in Nd:$GdVO_4$ and similar crystals and reported in elsewhere [15]–[17].

The related optical properties of Nd:$GdVO_4$ strongly depend on its lattice structure, which can be easily altered in an ion irradiation environment. In addition, the optical waveguides formed by structural changes in the Nd:$GdVO_4$ crystal can potentially to develop compact and efficient waveguide lasers and amplifiers. Considering the potential application of Nd:$GdVO_4$ in the optical field, ion irradiation leads to lattice structure changes, and subsequent changes in the related optical properties, which are of utmost importance.

Ion irradiation is a powerful and controllable method of changing the lattice structure in the near-surface, and it has been conducted on a variety of crystal materials. To the best of our knowledge, 1064 nm laser oscillation have been demonstrated and characterized in channel waveguides fabricated by carbon ions irradiation at a fluence of 8×10^{14} ions/cm^2 on Nd:YVO_4 using different output couplers [18]. The optical waveguide properties of Nd:$GdVO_4$ irradiated by triple-energy oxygen ions irradiation have also been characterized [19]. Here, we characterize the related optical properties of Nd:$GdVO_4$ irradiated by 460 keV H ions (light ion) at a fluence of 5.6×10^{16} ions/cm^2 and by 6.0 MeV C^{3+} ions (medium-mass ion) at fluences of 1.0×10^{15} ions/cm^2 and 3.0×10^{15} ions/cm^2. The dpa, XRD, hardness and elastic (Young's) modulus, and micro-Raman spectra were used to determine the lattice structure changes induced by different ion irradiation conditions. The related optical properties caused by the lattice structural change, including absorption spectra and refractive index, are investigated in this paper.

2. Experimental Details

Tetragonal single crystals of Nd:$GdVO_4$, with dimensions of 5.0 mm $\times$ 5.0 mm $\times$ 1.0 mm, were purchased from CASTECH INC.. H ion irradiation was carried out using an implanter at the Semiconductor Institute of the Chinese Academy of Sciences, and C^{3+} ion irradiation was performed at Peking University. The details of the ion-irradiated Nd:$GdVO_4$ crystals are shown in Table 1.

To study the near-surface structural changes of the ion-irradiated Nd:$GdVO_4$ crystal, the following properties were explored. The SRIM 2013 was used to calculate the dpa to describe the degree of damage of the ion-irradiated Nd:$GdVO_4$ crystals. A photograph of the irradiation cross-section was taken using a microscope (Axio Imager, Carl Zeiss) with transmitted polarized light. The structural characteristics of the samples were determined using a Bruker D8 Advance diffractometer equipped with a Cu $K_{\alpha 1}$ line ($\lambda = 0.15406$ nm) with a step size of $\Delta 2\theta = 0.04$ at the State Key Laboratory of Crystal Materials at Shandong University. The hardness and elastic (Young's) modulus profiles as functions of the depth were obtained using an Agilent Technologies G200 Nano Indenter. The

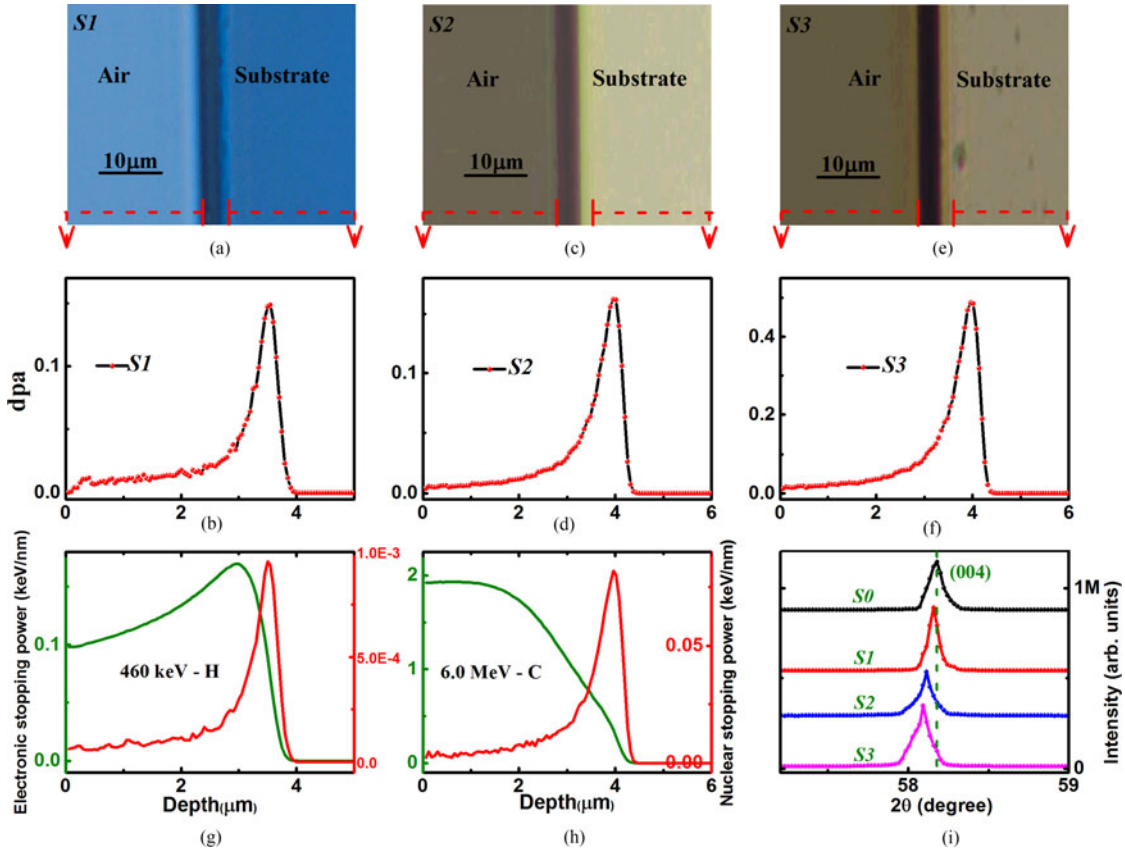

Fig. 1. Microscope cross-sectional photographs of the Nd:$GdVO_4$ crystals. (a) Sample *S1*, (c) sample *S2*, and (e) sample *S3*. The dpa distribution of the near- surface region. (b) Sample *S1*, (d) sample *S2*, and (f) sample *S3*. The electronic and nuclear stopping power as a function of the penetration depth. (g) 460 keV H ions and (h) 6.0 MeV C^{3+} ions irradiated into Nd:$GdVO_4$. (i) XRD pattern (θ-2θ) of the un-irradiated (sample *S0*) and irradiated Nd:$GdVO_4$ crystal (samples *S1*-*S3*).

confocal micro-Raman spectra of the samples were obtained using a HR800 Horiba/Jobin Yvon spectrometer. In our experiments, a laser source with a wavelength of 633 nm was used, and its spot size was $\leq$1 μm.

The related optical properties induced by the lattice structure changes were also investigated. The absorption spectra of the un-irradiated and irradiated samples were recorded using a Jasco U570 spectrophotometer. In addition, the optical-waveguide properties of the Nd:$GdVO_4$ crystals were characterized using prism coupling and end-face coupling techniques, and discussed using reflectivity calculation method (RCM).

3. Results and Discussion

To distinguish between the two different ion irradiations, by optimizing the color mode, the cross-sectional images of the polished ion-irradiated Nd:$GdVO_4$ crystals are shown in Fig. 1(a), (c), and (e). The images show that the depth of the modified layer is approximately 3.54 μm for sample *S1* and 4.02 μm for samples *S2* and *S3*. The dpa at damage peak are 0.15, 0.16, and 0.48 for samples *S1*, *S2*, and *S3,* which was simulated by SRIM 2013 and is displayed in Fig. 1(b), (d), and (f). The position of damage peak is in good agreement with the depth of the modified layer [as shown in Fig. 1(a), (c), and (e)]. To an extent, the dpa reflects the lattice structure changes and damage degree. The electronic and nuclear stopping power of 460 keV H and 6.0 MeV C^{3+} ions are

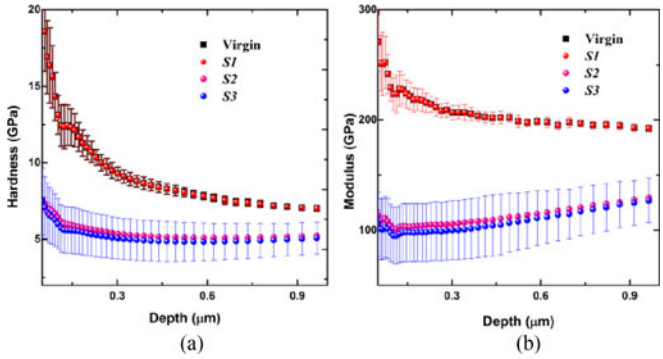

Fig. 2. (a) Hardness and (b) modulus versus indentation depth for samples *S0*-*S3*.

presented in Fig. 1(g) and (h). As we know, the H and C^{3+} ions lose most their energy by electronic ionizations(inelastic collisions) along their trajectory inside the Nd:$GdVO_4$ crystal, which results in the formation of colour centres and possibly damage in near-surface regions; the nuclear collisions (elastics collisions) bring about the reduction of physics density and a refractive-index decrease. In this paper, we compare the irradiation effects of Nd:$GdVO_4$ crystal irradiated by different kind of ions (medium-mass ion and light ion) with similar dpa, and we also compare the samples irradiated with different fluences by same kind of ion.

Fig. 1(i) presents the measured XRD patterns of the samples *S0*-*S3*. As evidence, the un-irradiated Nd:$GdVO_4$ samples show a diffraction peak at $2\theta = 58.1725^{o}$, which corresponds to the reflections from the (004) planes (ICSD card no. 15607) that belong to the (001) crystal plane family. The residual stress induced by ion irradiation causes lattice distortion, increases the lattice constant, and lead to a gradual left-shift in the diffraction peak for the irradiated samples *S1*, *S2*, and *S3*. The positions of the diffraction peak are $2\theta = 58.1509^{o}$, 58.1077^{o}, and 58.0869^{o} for samples *S1*, *S2*, and *S3*, respectively. The interplanar spacing was estimated using the Prague formula

$$2d \sin\theta = n\lambda \tag{1}$$

where d is the interplanar spacing, θ is the diffraction angle, n ($n = 4$) is the diffraction order, and λ is the X-ray wavelength. From the formula above, we can determine the mean interplanar spacings in the near-surface $d0 = 6.3383\mathring{A}$ (sample *S0*), $d1 = 6.3404\mathring{A}$ (sample *S1*), $d2 = 6.3447\mathring{A}$ (sample *S2*), and $d3 = 6.3468\mathring{A}$ (sample *S3*). The interplanar spacing for samples *S1*, *S2*, and *S3* changes by 0.0331%, 0.1009%, and 0.1341%, respectively, compared to the un-irradiated sample *S0*. The variation of the interplanar spacing reflects the degree of lattice distortion to a certain extent. Compared with the dpa [as shown in Fig. 1(b), (d) and (f)], C^{3+} ions irradiated on the Nd:$GdVO_4$ crystal brought out greater damage than H ion irradiated with the similar dpa.

The changes in the mechanical property induced by ion irradiation are also discussed. The hardness and elastic (Young's) modulus as continuous functions of the depth were obtained from samples *S0*- *S3* to determine the evolution of the mechanical property, as observed in Fig. 2. Due to the indentation size effect [20], the measured hardness for the un-irradiated sample (*S0*) decreased with increasing depth. Compared to sample *S0*, the hardness and elastic modulus of sample *S1* hardly changed, which indicates that the ion irradiation has little effect on the surface lattice structure for sample *S1*. Due to the irradiation effect, the surface roughness gradually increased for samples *S2* and *S3*, and the obvious decrease of the hardness is qualitatively confirmed in Fig. 2(a) [21]. Clearly, the elastic modulus gradually decreased for samples *S1*-*S3* due to ion irradiation. Based on the interatomic potential energy theory [22], the lattice damage, the decreased interatomic bond strength and density, and the increased atomic spacing (see Figs. 1, 3, and 4) lead to a decrease of the elastic modulus [as shown in Fig. 2(b)]. The hardness and elastic modulus results also show that C^{3+} ions irradiated on the Nd:$GdVO_4$ crystal brought out greater damage than H ions irradiated with similar dpa, and consistent with XRD and other results in the paper (see Figs. 1, 3, and 4).

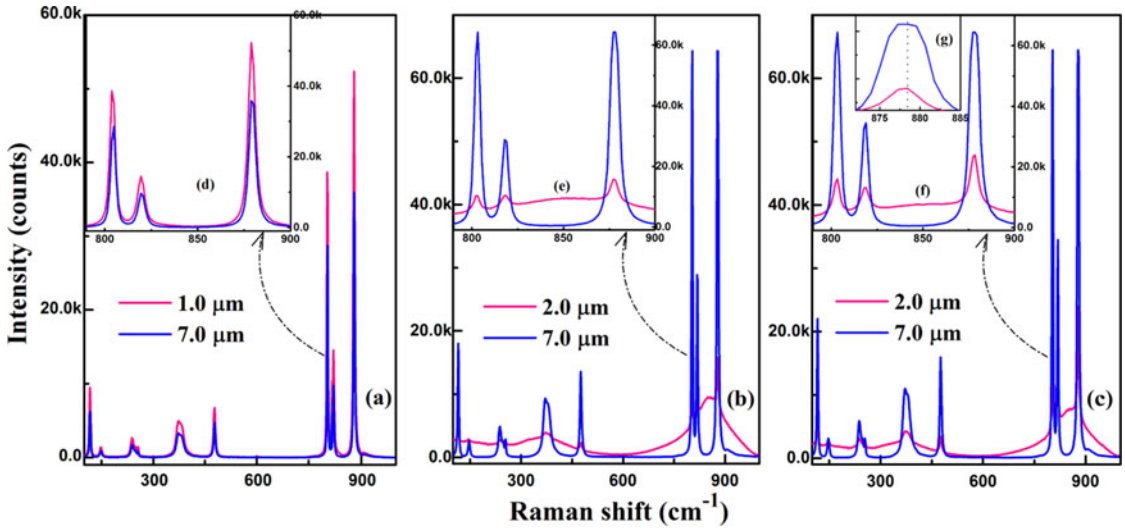

Fig. 3. Raman spectra obtained at the end face of the sample with different detection locations. Infrared irradiated region (1.0 or 2.0 μm) is labeled by the pink line, and the un-irradiated region (7.0 μm) is labeled by the blue line. (Inset) Magnified view of the Raman peaks at 808, 823, and 878 cm^{-1}. (a), (d) 460 keV H ions with a fluence of 5.6×10^{16} ions/cm^2. (b), (e) 6.0 MeV C^{3+} ions with a fluence of 1.0×10^{15} ions/cm^2. (c), (f), (g) 6.0 MeV C^{3+} ions with a fluence of 3.0×10^{15} ions/cm^2.

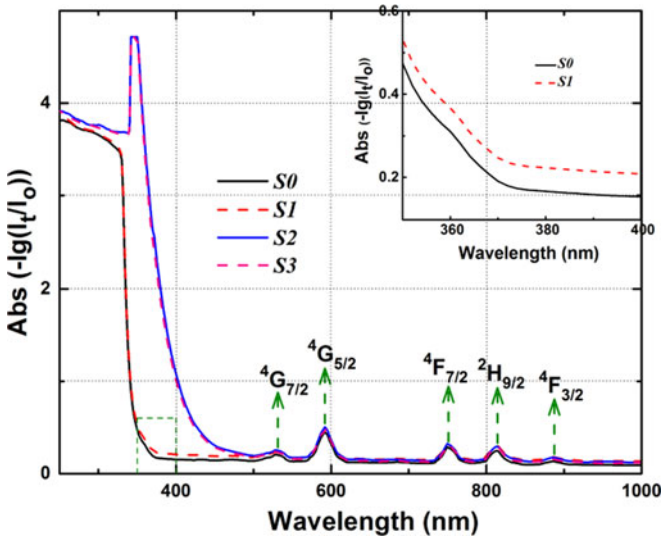

Fig. 4. Absorption spectra of Nd:$GdVO_4$ samples: the black, red, blue, and pink lines represent samples *S0*, *S1*, *S2*, and *S3*, respectively. The inset represents an enlarged view of the absorption spectra of samples *S0* and *S1* at a wavelength range from 350 to 400 nm.

Fig. 3 shows Raman scattering active modes of the samples at irradiated and un-irradiated region in a frequency range from 100 to 1000 cm^{-1}. The insets [see Fig. 3(d), (e), and (f)] represent magnified views of the three stronger peaks. The peaks shown in Fig. 3(g) correspond to the V-O stretching mode for sample *S3*. For the Nd:$GdVO_4$ crystal, the unit cell contains two VO_4^{3-} anions and two Gd^{3+}(or Nd^{3+}) cations, and the factor group analysis reveals that a total of 36 normal modes were classified as follows [23]:

$$\Gamma = 2A_{1g} + 1A_{1u} + 1A_{2g} + 4A_{2u} + 4B_{1g} + 1B_{1u} + 1B_{2g} + 2B_{2u} + 5E_g + 5E_u.$$

The Raman active vibrational modes are as follows:

$$\Gamma = 2A_{1g} + 4B_{1g} + 1B_{2g} + 5E_g.$$

Among these, $2A_{1g} + 2B_{1g} + 1B_{2g} + 2E_g$ ac$[VO4]^{3-}$ anion, and $2B_{1g} + 3E_g$ are external vibrations. Only 9 of 12 Raman active modes were observed in the Raman spectra we measured. Based on the Raman spectra analysis and the prediction from the lattice-dynamical calculations, the Raman bands at 380 and 878 cm^{-1} could be assigned to the A_{1g} mode, the bands at 122, 481, and 808 cm^{-1} could be assigned to the B_{1g} mode, the band at 260 cm^{-1} could be assigned to the B_{2g} mode, and the bands at 155, 245, and 823 cm^{-1} could be assigned to the E_g mode. The modes observed in the region from 250-1000 cm^{-1} are the internal vibrations of the $[VO4]^{3-}$ anion, and the modes observed at 122, 155, and 244 cm^{-1} are external vibrations. Among them, the Raman peak at 878 cm^{-1} could be assigned to the V-O stretching mode, and the peak at 380 cm^{-1} was assigned to the in-plane O-V-O bending vibration mode [24]. The peak intensity of the H ion irradiation region was about 45% stronger than that of the virgin region in Fig. 3(a). The enhancement of Raman intensity is due to the increase of the polarizability induced by H ion irradiation with high fluence. The phenomenon of the Raman signal enhancement may have great potential value in practical applications. As shown in Fig. 3(b) and (c), the C^{3+} ion irradiation process resulted in an obvious decrease of the peak intensity, which could be attributed to the increase of the lattice disorder in the range of irradiation for the Nd:$GdVO_4$ crystal. In Fig. 3(g), the positions of the Raman peak are 878.4 and 877.9 cm^{-1} for the un-irradiated and irradiated regions of sample *S3*. Compared with the un-irradiated region, the peak value is shifted by 0.5 cm^{-1} to the left. This occurs because ion irradiation leads to an increase in the interplanar spacing (volume expansion in the irradiated region). Then, the volume expansion leads to a longer bond length, and the bond strength is weakened. We believe that the increase in the bond length is the reason for peak shift to the left. In addition, due to the sensitivity limitation of Raman detection, the peak shift at 878 cm^{-1} for the un-irradiated and irradiated regions is not obvious for samples *S1* and *S2*. Based on these variations of the Raman spectra, we determine that appropriate ion irradiation conditions can change the Raman signal intensity and lattice structure. The micro-Raman spectra, hardness and elastic (Young's) modulus, XRD and dpa provide accurate information of the lattice structure changes induced by ion irradiation. The related changes in the optical properties caused by the lattice structure changes were investigated below.

To investigate the influence of the lattice structure change on light absorption characteristics, Fig. 4 shows the absorption spectra of un-irradiated and irradiated samples (*S0*-*S3*) at wavelengths from 250 to 1000 nm. The inset is a magnified view at the wavelength range from 350 to 400 nm for samples

S0 and *S1*. The spectral parameters can be calculated based on the Judd-Ofelt (JO) theory in the CGSE system of units [25]-[27], and the calculated line intensity and optical parameters of the absorption spectrum are listed in [25]. As shown in Fig. 4, for the un-irradiated sample (*S0*), we observe five absorption peaks at 530, 591, 751, 814, and 888 nm, which correspond to $^4G_{7/2}$, $^4G_{5/2}$, $^4F_{7/2}$, $^2H_{9/2}$, and $^4F_{3/2}$. The absorption coefficient can be calculated using the following formula:

$$\alpha = -\left(\ln \frac{I_t}{I_o}\right) \Big/ L. \tag{2}$$

In (2), α is absorption coefficient, I_o and I_t are the incident and outgoing optical powers, respectively, and L ($L = 0.1\ cm$) is the thickness of the sample. Based on the formula above and the measured absorption spectra, the absorption coefficient of sample *S0* at 814 nm is $\alpha = 5.6937$ cm. The measured absorption coefficients of Nd:$GdVO_4$ are compared with the values obtained from the JO theory. A good fit is obtained when the JO theory of parity-forbidden electric-dipole transitions of rare earth ions at sites lacking inversion symmetry is applied to the Nd:$GdVO_4$ crystal. Compared with the un-irradiated sample (*S0*), the absorption increased by approximately 23.69%, 1147.43%, and 1147.43% for samples *S1*, *S2*, and *S3* at the near-edge optical absorption (at 365 nm), which may be due to the lattice structure change in the near surface. In addition, there are an obvious absorption peaks (at 346 nm) in the ultraviolet band after irradiation by C^{3+} ions for samples *S2* and

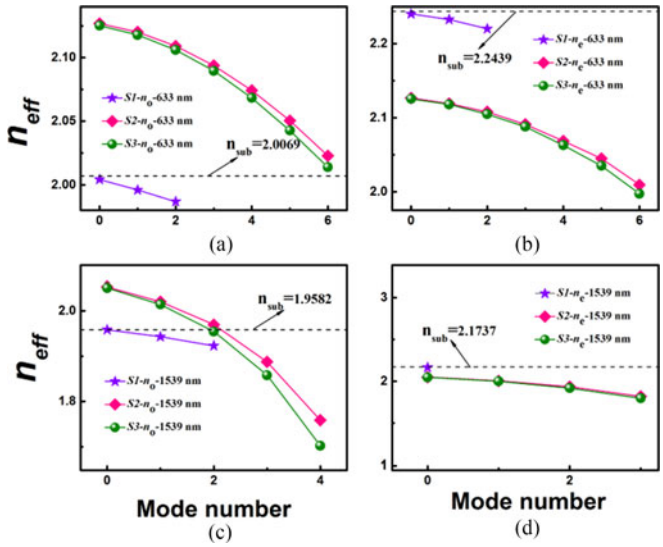

Fig. 5. Effective refractive index (n_{eff}) versus mode number of Nd:$GdVO_4$ crystals for n_o and n_e. (a), (b) At 633 nm. (c), (d) At 1539 nm.

S3. The results indicated that compared with sample *S0*, the larger lattice structure change caused by irradiation by C^{3+} ions led to the formation of a new absorption band. In addition, the absorption spectra in the visible and infrared bands are barely affected by ion irradiation. The introduction of a new absorption peak and the absence of changes in the visible and infrared bands are of significant importance in practical applications for the ion- irradiated Nd:$GdVO_4$ crystal.

The influence of the lattice structure changes on the refractive index is also explored, and the guided mode effective refractive indices (n_{eff}) of the Nd:$GdVO_4$ crystals are displayed in Fig. 5. The transverse electric (TE) modes of n_o at wavelengths of 633 and 1539 nm are shown in Fig. 5(a) and (c), respectively. The transverse magnetic (TM) modes of n_e at wavelengths of 633 and 1539 nm are shown in Fig. 5(b) and (d), respectively. The refractive indices measured before ion irradiation (n_{sub}) are also shown and represented by the black dashed line in Fig. 5. Clearly, the n_o increased and n_e reduced due to the reduction of spontaneous polarization by C^{3+} ion irradiation. In addition, n_o and n_e exhibit almost no change for H ion irradiation.

It can be observed from Fig. 5 that a suitable lattice structure change enables the formation of an optical waveguide structure. Therefore, the near-field light intensity profiles of the guided modes for Nd:$GdVO_4$ crystals were measured, and they are shown in Fig. 6(1). It is observed that sample *S1* has weaker ability to confine light than samples *S2* and *S3*, and sample *S1* exhibits significant light leakage. In addition, in the TE (n_o) mode, it is obvious that there is one- guided mode for sample *S1*, and there are two guided modes for samples *S2* and *S3*. In the TM mode, there is one guided mode for sample *S1*, there are two guided modes for sample *S2*, and there are three guided modes for sample *S3*. These experimental results were compared with the following simulated results [the inset of Fig. 6(2)] and verified. The propagation loss was measured by the back-reflection method [28], and the propagation loss is about 16.70, 3.00, and 2.5 dB/cm at 633 nm in the TE (n_o) mode for samples *S1*, *S2*, and *S3*, respectively; in addition, in the TM (n_e) mode, the propagation loss is about 3.45, 3.12, and 1.85 dB/cm at 633 nm for samples *S1*, *S2*, and *S3*, respectively. It is obvious that the relatively large lattice structure change in the near-surface region has a stronger ability to limit light propagation.

As shown in Fig. 1, the color within the ion-irradiated region is different from that within the substrate region, and this phenomenon is caused by the change of the refractive index in that region. From the *m*-line measurements of the guided mode (see Fig. 5), we reconstruct the RIP by applying RCM [29] at 633 nm; this is shown in Fig. 6(2). For the TE (n_o) mode, a positive ordinary

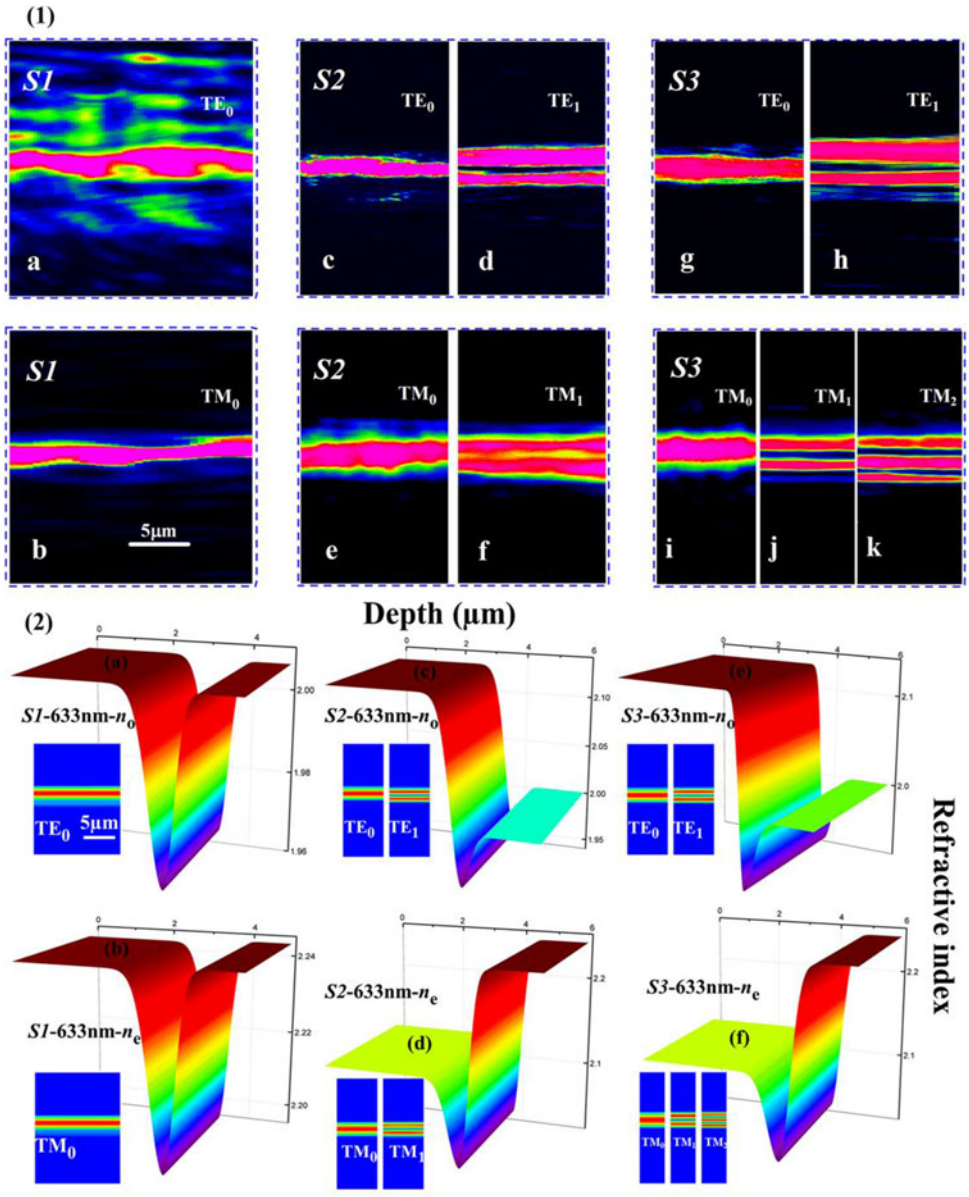

Fig. 6. (1) Modal profiles obtained from CCD camera data collection of guided modes at 633 nm. (2) 3-D reconstructed RIP from samples *S1*, *S2*, and *S3* at 633 nm. (Inset) Near-field light intensity profile simulated using the FD-BPM method.

index well was formed in the waveguide region, and the RIP is a typical "well + barrier" type, while the RIP for TM (n_e) is a pure "barrier" confined type. Clearly, the depth of the barrier is consistent with the peak position of dpa (see Fig. 1). The insets below the RIP represent the modal profiles, which were calculated using FD-BPM [30], according to the RIP; these profiles are compared with the experimental results [see Fig. 6(1)]. The consistency between the calculated and experimental results illustrates that the reconstructed RIP parameters were reasonable.

The thermal stability of samples *S1*, *S2*, and *S3* were investigated by continuous annealing treatments in an air atmosphere. The conditions for the annealing treatment are shown in Table 2.

For clarity, the n_{eff} of the TE_0 and TM_0 mode of the Nd:$GdVO_4$ crystals after different annealing treatment are shown in Fig. 7. After annealing at 260 C°C about 60min (T1), only in the TE (n_o)

TABLE 2
Details for Annealing ION-Irradiated Nd:$GdVO_4$ Samples in Air

Process	T0 (*S1*/*S2*/*S3*)	T1 (*S1*/*S2*/*S3*)	T2 (*S1*/*S2*/*S3*)	T3 (*S1*/*S2*/*S3*)
Annealing condition	As Irradiated	260 *C*°C for 60 min	T1 + 310 *C*°C for 60 min	T2 + 360 *C*°C for 60 min

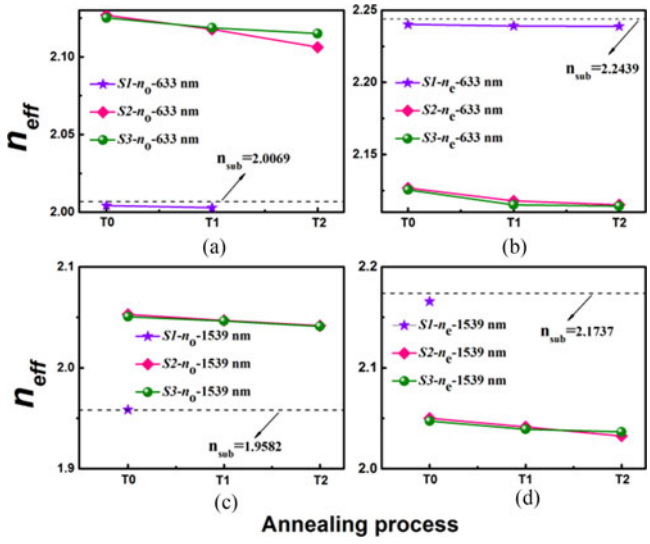

Fig. 7. Evolution of the n_{eff} versus annealing temperature for Nd:$GdVO_4$ crystal by ion irradiation at 633 and 1539 nm.

mode at 633 nm, the guided mode is present for sample *S1*; in addition, the guided mode is also disappeared for samples *S2* and *S3* after annealing at 360 *C*°C about 60 min (T3). From Fig. 7, the main feature of samples *S2* and *S3* is that the index is monotonically decreasing as annealing temperature increase. After annealing at 310 *C*°C for 60 min (T2), the propagation losses reduced to about 0.93 dB/cm and 0.70 dB/cm in the TE (n_o) mode at 633 nm for samples *S2* and *S3*; in addition, in the TM (n_e) mode, the propagation losses reduced to about 0.7 dB/cm and 0.54 dB/cm at 633 nm for samples *S2* and *S3*. For sample *S1*, the propagation is not reduced.

4. Conclusion

The related properties in the ion-irradiated Nd:$GdVO_4$ crystal have been studied using complementary characterization techniques. The dpa profile, the shift of the XRD diffraction peak, the hardness and elastic modulus and the micro-Raman spectra show the disorder of the lattice structure due to ion irradiation. The intensity and peak position of micro-Raman have obvious changes between waveguide and substrate region, and provide accurate information of the lattice structure changes induced by ion irradiation in Nd:$GdVO_4$ crystal. The investigation of the absorption spectra, refractive index profile, and the formation of the waveguide structure demonstrate that damage occurred on the samples. In addition, we can deduce that the near- surface lattice damage induced by C^{3+} ion (medium-mass ion) irradiation is higher than H ion (light ion) irradiation with similar dpa. Therefore, a reasonable choice of the irradiation ion, energy and fluence can effectively achieve changes in the related optical properties for the Nd:$GdVO_4$ crystal.

Acknowledgment

The authors would like to thank C. Xu for the ion irradiation on samples.

References

[1] J. E. Geusic, H. M. Marcos, and L. G. V. Uitert, "Laser oscillations in Nd-doped yttrium aluminum, yttrium gallium and gadolinium garnets," *Appl. Phys. Lett.*, vol. 4, no. 10, pp. 182–184, May 1964.
[2] T. Kushida, H. M. Marcos, and J. E. Geusic, "Laser transition cross section and fluorescence branching ratio for Nd^{3+} in yttrium aluminum garnet," *Phys. Rev.*, vol. 167, no. 2, pp. 289–291, Mar. 1968.
[3] F. Tan, F. X. Yu, and L. L. Wang, "Continuous-wave laser performance of an LD-end-pumped single Tm^{3+}–doped $GdVO_4$ crystal at room temperature," *J. Russ. Laser. Res.*, vol. 35, no. 3, pp. 295–297, May. 2014.
[4] Y. F. Ma, X. Yu, F. K. Tittel, and X. D. Li, "Diode-pumped continuous-wave and passively Q-switched 1.06 μm YVO_4/Nd:$GdVO_4$ laser," *Opt. Commun.*, vol. 285, pp. 1911–1914, 2012.
[5] Z. H. Li, J. Y. Peng, Y. Zheng, Y. Yang, and J. H. Kou, "C-cut Nd-doped vanadate crystal self-Raman laser with narrow Q-switched envelope and high mode-locked repetition rate," *Optoelectr. Lett.*, vol. 10, no. 6, pp. 423–426, Nov. 2014.
[6] A. Agnesi, A. Guandalini, G. Reali, S. Dell'Acqua, and G. Piccinno, "High-brightness 2.4-W continuous-wave Nd:$GdVO_4$ laser at 670 nm," *Opt. Lett.*, vol. 29, no. 1, pp. 56–58, Jan. 2004.
[7] Y. J. Yu *et al.*, "High repetition rate 880 nm diode-directly-pumped electro-optic Q-switched Nd: $GdVO_4$ laser with a double-crystal RTP electro-optic modulato," *Opt. Commun.*, vol. 304, pp. 39–42, 2013.
[8] E. J. Hao, T. Li, Z. D. Wang, and Y. Zhang, "Nd:$GdVO_4$ ring laser pumped by laser diode," *Laser Phys. Lett.*, vol. 10, no. 025803, 2013.
[9] A. I. Zagumennyi, V. G. Ostroumov, T. A. Shcherbarkov, T. Jensen, J. P. Meyn, and G. Huber, "The Nd:$GdVO_4$ crystal: A new material for diode-pumped lasers," *Sov. J. Quantum Electron.*, vol. 22, no. 12, pp. 1071–1072, Dec. 1992.
[10] T. Jensen *et al.*, "Spectroscopic characterization and laser performance of diode-laser-pumped Nd:$GdVO_4$," *Appl. Phys. B*, vol. 58, pp. 373–379, 1994.
[11] T. Ogawa *et al.*, "Efficient laser performance of Nd:$GdVO_4$ crystals grown by the floating zone method," *Opt. Lett.*, vol. 28, no. 23, pp. 2333–2335, Dec. 2003.
[12] V. Lupei, N. Pavel, Y. Sato, and T. Taira, "Highly efficient 1063-nm continuous-wave laser emission in Nd:$GdVO_4$," *Opt. Lett.*, vol. 28, no. 23, pp. 2366–2368, Dec. 2003.
[13] L. Fornasiero, S. Kück, T. Jensen, G. Huber, and B. H. T. Chai, "Excited state absorption and stimulated emission of Nd^{3+} in crystals. Part 2: YVO_4, $GdVO_4$, and $Sr_5(PO_4)_3F$," *Appl. Phys. B*, vol. 67, pp. 549–553, 1998.
[14] Y. F. Chen, "Efficient 1521-nm Nd:$GdVO_4$ Raman laser," *Opt. Lett.*, vol. 29, no. 22, pp. 2632–2634, Nov. 2004.
[15] Y. Tan, Y. C. Jia, F. Chen, J. R. V. Aldana, and D. Jaque, "Simultaneous dual-wavelength lasers at 1064 and 1342 nm in femtosecond-laser-written Nd:YVO_4 channel waveguides," *J. Opt. Soc. Amer. B*, vol. 28, no. 7, pp. 1607–1610, Jul. 2011.
[16] Y. Tan *et al.*, "70% slope efficiency from an ultrafast laser-written Nd:$GdVO_4$ channel waveguide laser," *Opt. Exp.*, vol. 18, no. 24, pp. 24994–24999, Nov. 2010.
[17] Y. Y. Ren *et al.*, "Continuous wave channel waveguide lasers in Nd:$LuVO_4$ fabricated by direct femtosecond laser writing," *Opt. Exp.*, vol. 20, no. 3, pp. 1969–1974, Jan. 2012.
[18] M. E. Sánchez-Morales *et al.*, "Laser emission in Nd:YVO_4 channel waveguides at 1064 nm," *Appl. Phys. B*, vol. 94, pp. 215–219, Nov. 2009.
[19] C. L. Jia, X. L. Wang, K. M. Wang, H. J Ma, and R. Nie, "Characterization of optical waveguide in Nd: GdVO4 by triple-energy oxygen ion implantation," *Appl. Surf. Sci.*, vol. 253, pp. 9311–9314, Jun. 2007.
[20] L. E. Samuels and T. O. Mulhearn, "An experimental investigation of the deformed zone associated with indentation hardness impressions," *J. Mech. Phys. Solids*, vol. 5, pp. 125–134, 1957.
[21] W. G. Jiang, J. J. Su, and X. Q. Feng, "Effect of surface roughness on nanoindentation test of thin films," *Eng. Fract. Mech.*, vol. 75, pp. 4965–4972, Jul. 2008.
[22] M. C. Osborne, J. C. Hay, L. L. Snead, and D. Steiner, "Mechanical- and physical-property changes of neutron-irradiated chemical-vapor-deposited silicon carbide," *J. Amer. Ceram. Soc.*, vol. 82, no. 9, pp. 2490–2496, Sep. 1999.
[23] P. Dawson, M. M. Hargreave, and G. R. Wilkinson, "The vibrational spectrum of zircon ($ZrSiO_4$)," *J. Phys. C: Solid State Phys.*, vol. 4, pp. 240–256, 1971.
[24] G. W. Lu, C. Li, W. C. Wang, Z. H. Wang, H. R. Xia, and P. Zhao, "Raman investigation of lattice vibration modes and thermal conductivity of Nd-doped zircon-type laser crystals," *Mater. Sci. Eng.*, vol. 98, pp. 156–160, 2003.
[25] H. D. Jiang *et al.*, "Optical and laser properties of Nd:$GdVO_4$ crystal," *Opt. Commun.*, vol. 198, pp. 447–452, Nov. 2001.
[26] W. T. Carnall, P. R. Fields, and B. G. Wybourne, "Spectral intensities of the trivalent lanthanides and actinides in solution. I. Pr^{3+}, Nd^{3+}, Er^{3+}, Tm^{3+}, and Yb^{3+}," *J. Chem. Phys.*, vol. 42, no. 11, pp. 3797–3806, Jun. 1965.
[27] W. F. Krupke, "Optical absorption and fluorescence intensities in several rare-earth-doped Y_2O_3 and LaF_3 single crystals," *Phys. Rev.*, vol. 145, no. 1, pp. 325–337, May 1966.
[28] L. Zhang *et al.*, "Low propagation loss of single-mode planar waveguides on MgF_2 crystals," *J. Lightwave. Technol.*, vol. 33, no. 11, pp. 2228–2232, Jun. 2015.
[29] P. J. Chandler and F. L. Lama, "A new approach to the determination of planar waveguide profiles by means of a nonstationary mode index calculation," *Opt. Acta.*, vol. 33, no. 2, pp. 127–143, 1986.
[30] D. Yevick and W. Bardyszewiski, "Correspondence of variational finite-difference (relaxation) and imaginary-distance propagation methods for modal analysis," *Opt. Lett.*, vol. 17, no. 5, pp. 329–330, Mar. 1992.